NEOPLASIA
www.neoplasia.com
Volume 23 Number 4 April 2021 pp. 439–455

Original Research

Transcriptional signatures underlying dynamic phenotypic switching and novel disease biomarkers in a linear cellular model of melanoma progression

Diogo de Oliveira Pessoa[a]; Flávia Eichemberger Rius[b]; Debora D'Angelo Papaiz[b]; Ana Luísa Pedroso Ayub[b]; Alice Santana Morais[b]; Camila Ferreira de Souza[b]; Vinicius Ferreira da Paixão[a]; João Carlos Setubal[a]; Julia Newton-Bishop[c]; Jérémie Nsengimana[c,1]; Hatylas Azevedo[d]; Eduardo Moraes Reis[a,*]; Miriam Galvonas Jasiulionis[b,*]

[a] Departamento de Bioquímica, Instituto de Química, Universidade de São Paulo, São Paulo, Brazil
[b] Pharmacology Department, Universidade Federal de São Paulo, São Paulo, Brazil
[c] Institute of Medical Research at St James's, University of Leeds, Leeds, UK
[d] Division of Urology, Department of Surgery, Universidade Federal de São Paulo, São Paulo, Brazil

Abstract

Despite advances in therapeutics, the progression of melanoma to metastasis still confers a poor outcome to patients. Nevertheless, there is a scarcity of biological models to understand cellular and molecular changes taking place along disease progression. Here, we characterized the transcriptome profiles of a multi-stage murine model of melanoma progression comprising a nontumorigenic melanocyte lineage (melan-a), premalignant melanocytes (4C), nonmetastatic (4C11-) and metastasis-prone (4C11+) melanoma cells. Clustering analyses have grouped the 4 cell lines according to their differentiated (melan-a and 4C11+) or undifferentiated/"mesenchymal-like" (4C and 4C11-) morphologies, suggesting dynamic gene expression patterns associated with the transition between these phenotypes. The cell plasticity observed in the murine melanoma progression model was corroborated by molecular markers described during stepwise human melanoma differentiation, as the differentiated cell lines in our model exhibit upregulation of transitory and melanocytic markers, whereas "mesenchymal-like" cells show increased expression of undifferentiated and neural crest-like markers. Sets of differentially expressed genes (DEGs) were detected at each transition step of tumor progression, and transcriptional signatures related to malignancy, metastasis and epithelial-to-mesenchymal transition were identified. Finally, DEGs were mapped to their human orthologs and evaluated in uni- and multivariate survival analyses using gene expression and clinical data of 703 drug-naïve primary melanoma patients, revealing several independent candidate prognostic markers. Altogether, these results provide novel insights into the molecular mechanisms underlying the phenotypic switch taking place during melanoma progression, reveal potential drug targets and prognostic biomarkers, and corroborate the translational relevance of this unique sequential model of melanoma progression.

Neoplasia (2021) 23, 439–455

Keywords: Melanoma, Malignancy, Metastasis, EMT, Phenotype switch, Prognosis

Abbreviations: AJCC, American Joint Committee on Cancer; EMT, Epithelial-to-Mesenchymal Transition; DEGs, Genes Differentially Expressed; GEO, Gene Expression Omnibus; GO, Gene Ontology; MSS, Melanoma Specific Survival; NSG, Next-Generation Sequencing; PCA, Principal Component Analysis.

* Corresponding authors.
E-mail addresses: emreis@iq.usp.br (E.M. Reis), mgjasiulionis@unifesp.br (M.G. Jasiulionis).
[1] Present address: Biostatistics Research Group, Population Health Sciences Institute, Newcastle University, Newcastle

Received 14 January 2021; received in revised form 21 February 2021; accepted 12 March 2021

https://doi.org/10.1016/j.neo.2021.03.007

Introduction

Melanoma is the most lethal type of skin cancer, being responsible for nearly 75% of all skin cancer deaths. The overall incidence and mortality of this disease continue to increase worldwide, especially in the fair-skin population. When detected early, cutaneous melanoma is usually cured by surgery; however, progression to advanced or metastatic stages leads to tumors refractory to current chemo/radiotherapies, due to the accumulation of genetic/epigenetic changes and clonal selection [1]. Thus, a deeper understanding of the molecular basis of melanoma cell progression, plasticity and heterogeneity may reveal new ways to eliminate tumor subpopulations with aggressive behavior, and identify novel biomarkers for the diagnosis and prognosis of this lethal disease.

Next-generation sequencing (NGS) studies using both murine and human cell lines and tissue specimens have provided vast information about somatic, transcriptional and epigenetic changes that occur in melanoma, contributing substantially to the knowledge about its molecular basis [2,3]. More recently, several transcriptome studies based on patient-derived cell lines (Tsoi et al., 2018) or single cell RNA sequencing of either human samples or animal genetic models have revealed different phenotypic states contributing to intratumoral melanoma heterogeneity, especially in the context of drug response (Rambow et al., 2018; Tirosh et al., 2019; Baron et al., 2020). However, the sequential molecular events involved in melanocyte malignant transformation remain poorly understood [4], especially due to the scarcity of experimental linear models that could recapitulate the steps involved in the initiation and progression of melanoma.

To fill this gap, our group has established a 4-stage murine model of melanocyte malignant transformation by subjecting the melanocyte lineage melan-a [5] to sequential cycles of forced anchorage impediment (de-adhesion), a sustained stressful condition. Initially, a cell line corresponding to nontumorigenic premalignant melanocytes (4C) was obtained after subjecting melan-a cells to 4 cycles of adhesion impediment. Next, a nonmetastatic but tumorigenic slow-growing melanoma cell line (4C11-) was obtained after the limiting dilution of spheroids formed by 4C adhesion impediment. Lastly, a metastasis-prone and tumorigenic fast-growing melanoma cell line (4C11+) was obtained following spontaneous loss of p53 expression in 4C11- cells. This linear cellular model of melanoma progression has the important advantage that the tumorigenic cell lines could be used *in vivo* to grow tumors in immunocompetent mice [6-8].

Here we have employed RNA sequencing to investigate the transcriptome profiles of these cell lines and gain insights into the molecular and functional changes taking place from the initial steps of melanocyte malignant transformation to the late stages of melanoma progression. Gene expression signatures associated with malignancy, metastasis and epithelial-to-mesenchymal transition (EMT) were identified, revealing a dynamic phenotypic and transcriptional switch during melanoma progression that resembles cellular states described along the human melanoma differentiation trajectory [9]. These signatures have revealed well-known genes altered in human melanoma as well as novel genes whose expression was functionally annotated in the sequential context of tumor progression. Moreover, several deregulated genes were identified as independent prognostic factors in human melanoma patients, corroborating the translational relevance of this model.

Methods

Cellular model of melanoma progression

The murine model of melanoma progression has been previously described [6-8,10-14] and comprises spontaneously immortalized nonmalignant melanocytes (melan-a) [5] and 3 cell lines with increasing malignant potential (4C, 4C11- and 4C11+) derived from melan-a following sequential cycles of forced anchorage impediment. Briefly, *anoikis*-resistant yet still nontumorigenic cells (named 4C) were obtained after subjecting melan-a melanocytes to 4 cycles of de-adhesion/adhesion. Each cycle was achieved by maintaining cells into agarose-coated plates for 96h followed by culture in normal adhesion conditions. After submitting 4C cells to an additional de-adhesion cycle, the formed spheroids were subjected to a limiting dilution, clones were randomly selected and expanded to generate tumorigenic melanoma cell lines (as 4C11-). A metastatic 4C11+ cell line was obtained after the expanded nonmetastatic 4C11- cell line spontaneously lost p53 protein. After established, all cell lines were maintained in normal adherent conditions. Melan-a cells were cultured in RPMI (pH 6.9; Gibco, Carlsbad, CA), supplemented with 5% fetal bovine serum (Gibco) at 37°C in a humidified atmosphere of 5% CO_2 and 95% air, in the presence of 200 nM 12-*o*-tetradecanoylphorbol-13-acetate (PMA; Tocris, Ellisville, MO), required for melanocytes to survival and proliferate in culture [5]. The melanoma cell lines derived from melan-a cells were cultured in the same conditions, without PMA, since melanoma cells do not require the activation of protein kinase C signaling to proliferate.

RNA isolation, NGS library preparation and sequencing

Each of the 4 cell lines was plated in triplicate and cultured until 70% to 80% sub confluence. RNA was isolated from the same number of cells (10^7) using TRIzol reagent according to the manufacturer's protocol (Thermo Fisher Scientific Inc.) and treated with RNAse-free DNAse. Integrity was assessed by capillary electrophoresis in a BioAnalyzer instrument (Agilent Technologies, Inc.). Next, cDNA libraries were prepared with Illumina TruSeq Stranded Total RNA Library Prep Kit with Ribo-Zero Gold for depletion of ribosomal RNA (cat. # RS-122-2001, Illumina Inc.) using 1 μg of total RNA and following the manufacturer's protocol. The prepared cDNA libraries were quantified with KAPA Library Quantification Kit (cat. # KK4835, Roche Inc.) and pair-end sequenced (2 × 100nt) in a HiSeq 1500 platform (Rapid SBS Kit v2 - 200 Cycle, Illumina Inc.).

RNA-seq data acquisition and preprocessing

Quality control and adaptor trimming was conducted with Fast-QC [15] and Trimmomatic [16], respectively, using default parameters. Next, the RNA sequencing data was mapped to the annotated mouse genome (Ensembl 90 version) using the STAR aligner [17]. Reads mapped to gene annotations were quantified and summarized using the *Rsubread* R package [18]. One replicate library from melan-a was discarded due to the low percentage of reads mapping to the reference genome. Genes with read counts less than 1 CPM (count per million) in at least 4 out of 11 libraries (35% of samples) were discarded; expression values of the remaining genes were normalized and log transformed through the *voom* function from the *limma* R package [19]. Raw and processed sequence data is available at GEO (Gene Expression Omnibus) under accession GSE149884.

Gene expression data analysis

Principal component analysis (PCA) was performed with the R *prcomp* function. Hierarchical clustering using the Euclidean distance was carried with *heatmap.2* function. The results were visualized with ggplot2 [20]. Normalized expression data from the 4 cell lines was used to perform pairwise comparisons and identify differentially expressed genes in each cell type using the *limma* R package [19]. A significance threshold of log2 ratio $\geq |2|$ and Benjamini-Hochberg adjusted *P*-value ≤ 0.01 were used. The intersection among the genes differentially expressed in each pairwise comparison was evaluated using the *Venn* function. Lists of differentially expressed genes in each pairwise comparison were tested for enrichment of specific biological terms. We used the *gprofileR* package with a "moderate" hierarchical filter to obtain meaningful Gene Ontology (GO) terms for

biological processes [21], as well as the clusterProfiler and *limma* R packages [19] for Gene Ontology and KEGG Pathway analysis. A significance threshold of adjusted $P \leq 0.05$ was used for the functional enrichment analysis. To search for the overlap between markers from a stepwise human melanoma differentiation trajectory proposed by Tsoi et al. (2018) [9] and the differential transcriptome profiles belonging to each cell line and transition stage in our model, we have extracted the markers and proposed categories (undifferentiated, undifferentiated-neural-crest-like, neural-crest-like, neural-crest-like-transitory, transitory-melanocytic and melanocytic) described in Table S3 from Tsoi and colleagues (2018) [9]. These human markers were mapped to their murine orthologs via BioMart and then searched in the RNAseq data from our murine cellular model of melanoma progression, to compare their differential expression across the cell lines and the frequency of up and downregulated markers from specific differentiation categories.

Microarray gene expression data acquisition and analysis

Total RNA from 3 additional independent cell cultures from each murine melanoma progression model stage was obtained as described above and used to generate labeled targets for expression oligoarray hybridization. Affymetrix Mouse 430_2.0 Arrays were used following the manufacturer's recommendations. RNA probe intensities were preprocessed, normalized and $\log_2$ transformed with the *expresso* function from the Affy R package [22]. For probe annotation, probe id information was converted to Entrez genes using the R package *AnnotationDbi* [23].

Gene expression validation by RT-qPCR

RNA was isolated from cell cultures using TRIzol (Invitrogen, Carlsbad, CA), and used for cDNA synthesis using QuantiTect Reverse Transcription Kit (QIAGEN, Dusseldorf, Germany), following the manufacturer' protocol. Equal amounts of each cDNA synthesized were used in qPCR in a Corbett Rotor-Gene 6000 detection system with a Fast Rotor-Gene SYBR Green PCR Master Mix (Qiagen, Dusseldorf, Germany). Specific primers for *Nqo1, Arnt2, Zbtb16, Kit, Snai2, Tyr, Twist1, Twist2, Zeb1, Mitf, Mlana, Tyrp1, Dct, Dlx4, Actb* and *Gapdh* (Table S1) were used in the final concentration of 0.4 μM. Relative expression of target genes was calculated by the $2^{-\Delta\Delta Ct}$ method using *Gapdh* or *Actb* as endogenous reference controls. The expression of *Cdkn2a* and *Cdkn2b* genes was evaluated by semi-quantitative RT-PCR, where cDNAs were amplified by endpoint PCR using specific primers (Table S1). PCR fragment amplification was confirmed by agarose gel staining with ethidium bromide.

Patient survival analysis

Differentially expressed murine genes were mapped to their human orthologs via *BioMart* and their tumor expression was analyzed for association with melanoma specific survival (MSS) in 703 primary melanoma patients of the Leeds Melanoma Cohort (European Genome-Phenome Archive accession number EGAS00001002922) [24]. For each orthologue gene, patients were grouped into "low" or "high" expression based on the median expression of the gene in all samples and Cox proportional hazards regression was used to test the association with MSS in 3 types of analyses: firstly univariably, secondly with adjustment of age, sex, and anatomical site and thirdly adjusting these factors plus the AJCC (American Joint Committee on Cancer) stage and mitotic rate. These analyses were conducted in STATA v14 (StataCorp, Texas, USA).

Results

Transcriptional landscape changes along the cellular model of melanoma progression

To explore molecular mechanisms underlying melanocyte malignant transformation and melanoma progression, we investigated gene expression changes in our 4-stage murine cellular model, consisting of nontumorigenic melanocytes (melan-a), nontumorigenic premalignant melanocytes (4C), nonmetastatic tumorigenic melanoma cells (4C11-), and metastatic tumorigenic melanoma cells (4C11+). The cell lines in this model display distinct phenotypic characteristics that are summarized in Table S2. For instance, while the melan-a and 4C11+ cells present a differentiated phenotype, the 4C and 4C11- cell lines have mesenchymal morphology. Moreover, only the 4C11+ displays a high proliferation rate and potential to form lung metastasis in vivo. For each cell line, RNA-seq data was generated (an average of 7 million paired-end mapped reads per cell, in triplicate) and, following data processing and filtering, the expression of 13,511 genes was detected in at least one cell type. These comprised 11,983 protein-coding genes, as well as different classes of noncoding RNAs (see **Table S3**).

We have initially applied unsupervised classification methods to search for underlying patterns of gene expression across the cell lines. Using Principal Component Analysis (PCA) (**Fig. 1A**) or hierarchical clustering (**Fig. 1B**), we observed that replicates were grouped together, demonstrating the technical reproducibility of the gene expression measurements. Notably, the PCA plots using the first two principal components (**Fig. 1A**) and the hierarchical clustering analysis (**Fig. 1B**) have grouped the cell lines matching their differentiated (melan-a and 4C11+) or "mesenchymal-like" (4C and 4C11-) morphology [8], pointing to the existence of specific gene expression alterations associated with these phenotypes.

Then, we have searched for transcriptional changes occurring throughout melanoma progression by pairwise comparisons of the expression profiles of nontumorigenic melanocytes (melan-a), premalignant (4C), tumorigenic (4C11-) and metastatic (4C11+) cell lines (**Fig. 1C**). Differentially expressed genes (DEGs) in each pairwise comparison are shown in **Figure 1D** and **Figure S1**. A gene set enrichment analysis was performed to identify potential biological processes and molecular pathways overrepresented by these genes (**Fig. 1E**). Hundreds of genes (n=914) were deregulated in premalignant 4C cells compared to melan-a melanocytes; they were associated with signaling pathways (MAPK, PI3K-Akt, Hippo, Ras) that promote increased cell migration and reduced cell differentiation/apoptosis. Notably, fewer genes (n=95) were deregulated in the transition from 4C to malignant 4C11- cells, which were mainly involved in the activation of focal adhesion and PI3K-AKT signaling. A large number of DEGs (n=1673) was identified between nonmetastatic 4C11- and metastatic 4C11+ cells, among which there were genes from signaling pathways altered in the transition between premalignant 4C cells and melan-a melanocytes that were modulated in the opposite direction (**Fig. 1E**). A complete list of the DEGs along the melanoma progression model is shown as supplementary material (**Table S4**).

To further validate the DEGs identified in the RNA-seq analysis, we have compared these DEGs with those previously identified after measuring gene expression changes from 3 independent replicate cell cultures using Affymetrix oligonucleotide microarrays [7]. Except for one comparison, we have found a statistically significant overlap between DEGs detected by each platform (Fisher's exact test P-value ranging from 2.2e-16 to 0.019, **Figure S2**). The overall greater number of DEGs exclusively detected in the RNA-seq analysis is likely due to the unbiased transcriptome coverage and greater sensitivity of this technique compared to oligonucleotide microarrays.

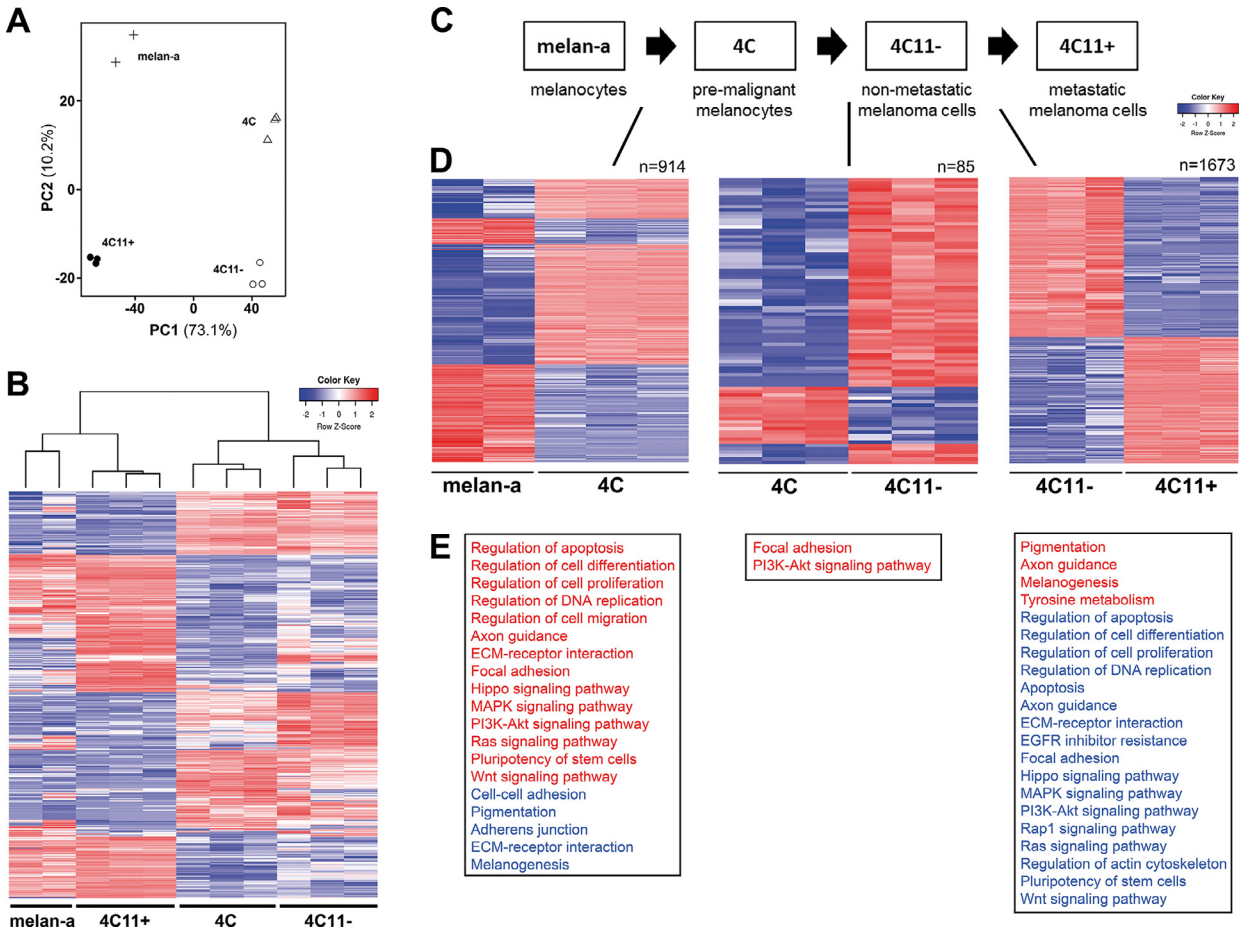

Fig. 1. Transcriptional changes along the murine melanoma progression model. Unsupervised analysis of gene expression data in cell lines representing different stages of melanoma progression showing the 500 most variable genes (median absolute deviation) between nonmalignant melan-a melanocytes, premalignant 4C melanocytes, nonmetastatic 4C11- and metastatic 4C11+ melanoma cell lines served as input for (**A**) Principal Component Analysis, and (**B**) Euclidean distance unsupervised clustering. (**C**) Schematic illustration of murine model of melanoma progression. (**D**) Differentially expressed genes (DEGs) along the melanoma progression were identified by pairwise comparison of cell lines with increasing malignancy using a significance threshold of log2 ratios $\geq |2|$ and Benjamini-Hochberg adjusted *P*-value ≤ 0.01. Heatmaps represent z-score normalized expression values of up (red) and downregulated (blue) genes relative to the average expression in each pair of cell lines. (**E**) Enriched biological processes among DEGs in each step of the tumor progression. Activated processes are in red whereas repressed processes are in blue.

Identification of molecular signatures related to malignancy, metastasis, and epithelial-to-mesenchymal transition (EMT)

Venn diagrams were constructed using the lists of DEGs in each pairwise comparison to identify transcriptional signatures associated with malignancy, metastasis and EMT. The malignancy signature was defined as the subset of 116 DEGs commonly deregulated in premalignant (4C) and tumorigenic (4C11- and 4C11+) cell lines compared to melan-a melanocytes. From those, 89 genes were found as differentially expressed in the same direction, i.e., consistently up- or downregulated in 4C, 4C11- and 4C11+ compared to melan-a (**Fig. 2A-C, Table S5**). Genes comprising this malignancy signature were enriched for biological functions related to cell migration, embryonic development and morphogenesis (**Fig. 2D**). This signature includes the gene coding for the receptor tyrosine kinase KIT, which was downregulated throughout the model of tumor progression (range $\log_2$ FC -9.9 to -3.5), in agreement with its tumor suppressor role in human melanoma [25]. Another downregulated gene was *Snai2* (*Slug*) ($\log_2$ FC -6.6 to -2.8), a master regulator of neural crest cell specification and migration. Conversely, *Nqo1*, which encodes the NAD(P)H quinone oxidoreductase 1, was upregulated particularly in the 4C and 4C11- cells ($\log_2$ FC 3.6 to 5.5). For independent confirmation, the transcriptional changes of *Kit, Snai2* and *Nqo1* genes initially detected by RNA-seq were validated by RT-qPCR. These results have demonstrated the statistically significant downregulation of *Kit* (**Fig. 2E**) and *Snai2* (**Fig. 2F**) and the upregulation of *Nqo1* (**Fig. 2G**) in premalignant and tumorigenic cell lines compared to melan-a melanocytes.

To identify a metastasis signature in the melanoma progression model, we have searched for common DEGs among the different pairwise comparisons between each nonmetastatic cell line (melan-a, 4C and 4C11-) and the metastatic cell line (4C11+) (**Fig. 3A**). The intersection between the lists of DEGs from each comparison is shown in **Figure 3B**. A subset of 347 DEGs was found to be consistently up or downregulated in 4C11+ metastatic cells compared to melan-a, 4C and 4C11- cell lines, being 332 in the same direction (**Fig. 3C, TABLE S6**). This metastasis signature contains genes enriched for several biological processes related to cancer, including cell adhesion, migration, differentiation and development (**Fig. 3D**). Among the genes downregulated in the metastatic cell line, *Cdkn2a* ($\log_2$ FC -9.2 to -8.5) and *Cdkn2b* ($\log_2$ FC -7.6 to -7.0) encode important cell cycle inhibitors whose expression is frequently lost or inactivated in melanomas [26]. *Zbtb16* (zinc finger and BTB domain containing 16), also known as *Plzf*, was also downregulated in 4C11+ cells ($\log_2$ FC -5.5 to -4.5); it encodes

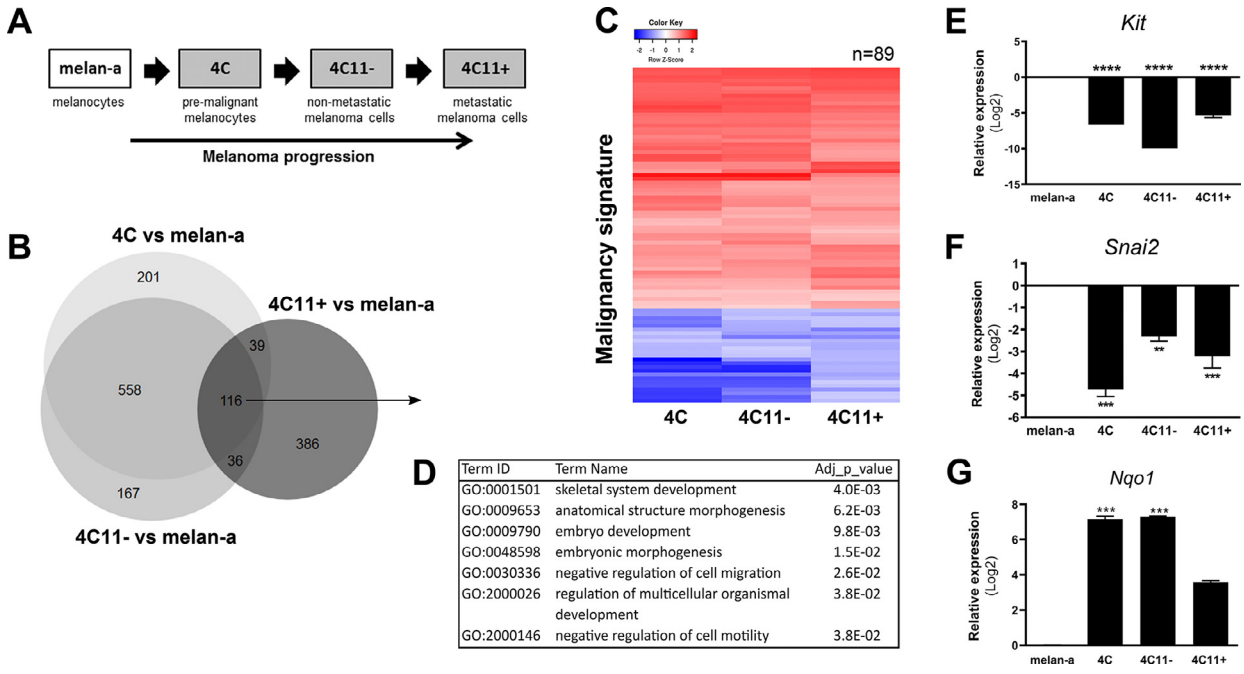

Fig. 2. A malignancy signature of melanoma progression. (**A**) Progression model schema from nonmalignant melanocytes (in white) to transformed cells with increasing malignancy (in gray). (**B**) Venn diagram with DEGs in pairwise comparisons between premalignant 4C, nonmetastatic 4C11- and metastatic 4C11+ melanoma cell lines to nonmalignant melan-a melanocytes (log2 ratios $\geq |2|$ and Benjamini-Hochberg adjusted *P*-value ≤ 0.01). (**C**) Heatmap with z-score normalized expression values of 89 DEGs detected in all malignant cells lines compared to nonmalignant melan-a melanocytes (upregulated genes in red, downregulated genes in blue) (**D**) Enriched biological processes and molecular pathways categories in the 89-gene malignancy signature. (**E-G**) Relative expression levels of *Kit, Snai2* and *Nqo1*, respectively, in the cell lines determined by RT-qPCR (see Methods for details).

a transcriptional repressor that maintains stem/progenitor cells in a quiescent state. Other genes found in this metastasis signature include *Cdkn1a* (log_2 FC 4.2 to 4.4), *Tyr* (log_2 FC 7.9 to 11.9), *Arnt2* (log_2 FC 4.5 to 7.2), *Mdm2* (log_2 FC 2.3 to 2.5), *Gpr143* (log_2 FC 2.1 to 8.5), *Rab38* (log_2 FC 4.0 to 11.7), *Angpt2* (log_2 FC 3.3 to 3.9), *Mgat5* (log_2 FC 2.3 to 2.5), *Pou4f1* (log_2 FC 3.6 to 5.4) and *Six1* (log_2 FC 3.5 to 7.3) (**Table S6**).

An independent analysis confirmed that the genes encoding cyclin-dependent kinase inhibitors 2A (*Cdkn2a*) (**Fig. 3E**) and 2B (*Cdkn2b*) (**Fig. 3F**) showed lower expression in the metastatic (4C11+) cell line, the gene coding for Zinc finger and BTB domain-containing protein 16 *(Zbtb16)* had reduced expression in metastatic compared to mesenchymal cells (**Fig. 3I**), whereas the tyrosinase (*Tyr*) (**Fig. 3G**) and *Arnt2* genes (**Fig. 3H**) were upregulated in 4C11+ cells compared to melanocytes, premalignant and tumorigenic cells. These expression changes were confirmed by RT-qPCR or semi-quantitative endpoint RT-PCR (**Fig. 3G-I,** and **Fig. 3E-F**, respectively).

The finding that the gene expression profiles of the cell lines with differentiated and mesenchymal-like phenotypes [8,27] clustered together in our model (**Fig. 1**, **A** and **B**) has prompted us to explore a transcriptomic signature associated with EMT (**Table S2**). To this end, we have performed a differential expression analysis comparing the differentiated melan-a and 4C11+ cells with the "mesenchymal-like" 4C and 4C11- cells (**Fig. 4A**). A total of 1200 DEGs ($p_{adj} < 0.01$) were identified (**Fig. 4B, Table S7**). Genes upregulated in "mesenchymal-like" cells were enriched for biological processes and signaling pathways relevant to EMT, such as WNT, RAS, PI3K-AKT, TGF-beta, and MAPK pathways, whereas downregulated DEGs displayed enriched functions involved in focal adhesion and axon guidance (**Fig. 4B**). Among these genes, *Snai1* ($log_2FC = 7.1$), *Twist1* ($log_2FC = 4.7$), *Twist2* ($log_2FC = 7.3$), *Zeb1* ($log_2FC = 6.0$) and *Dlx4* ($log_2FC = 6.1$) were upregulated in mesenchymal-like cells. The latter gene was shown to induce EMT by upregulating Twist, promoting migration and invasiveness in breast cancer cells [28]. Several other upregulated genes in the "mesenchymal-like" cell lines are involved with a cancer stem cell phenotype, such as *Sox9, Tgfb3, Gli1, Gli2, Notch3, Cd24a, Igf1, Klf5, Gas1, Gas6, Ror1, Cited1* and *Arid3b,* or with adaptive responses following drug treatment, such as *Gfra1, Bmp4, Dlx5,* and *Bgn* (**Table S7**). In parallel, genes previously associated with highly proliferative and differentiated melanoma cells (*Mitf, Mlana*), pigmentation (*Tyrp1, Dct, Gpr143*) and a transmembrane protease and MYC target (*Psen2*) were downregulated in "mesenchymal-like" cells ($log_2FC = -7.3$, -10.6, -12.4, -12.0, -3.1 and -7.3, respectively). The expression of *Sox10*, a neural crest marker required for melanoma cell proliferation and differentiation [29], was also decreased in 4C and 4C11- cell lines ($log_2FC = -10.0$) (**Table S7**). The upregulation of *Twist1, Twist2, Zeb1* and *Dlx4*, and the downregulation of *Mitf, Tyrp1, Mlana* and *Dct* in the mesenchymal-like cells were independently validated by RT-qPCR (**Fig. 4C**).

Expression patterns of stage markers of human melanoma differentiation in our linear model of melanoma progression

Tsoi et al. (2018) [9] have proposed a multi-stage differentiation model for human melanoma after clustering gene expression profiles from 53 human melanoma cell lines. They have identified genes that were either differentially expressed (DE) specifically at one of the 4 progressive stages (undifferentiated, neural crest-like, transitory and melanocytic), or that had shared differential expression between 2 adjacent subtypes in the differentiation model (undifferentiated-neural crest-like, neural crest-like-transitory and transitory-melanocytic). To check if our linear melanoma progression model recapitulates the phenotypic states seen during the human melanoma differentiation trajectory, we evaluated the expression patterns of the markers from each differentiation stage in the murine cell lines. **Figure 5A** displays the average expression values of murine orthologs of genes belonging to each subtype or to 2 adjacent subtypes across the cell lines from our model. Interestingly, the 4C and 4C11- "mesenchymal-like" cell lines exhibited

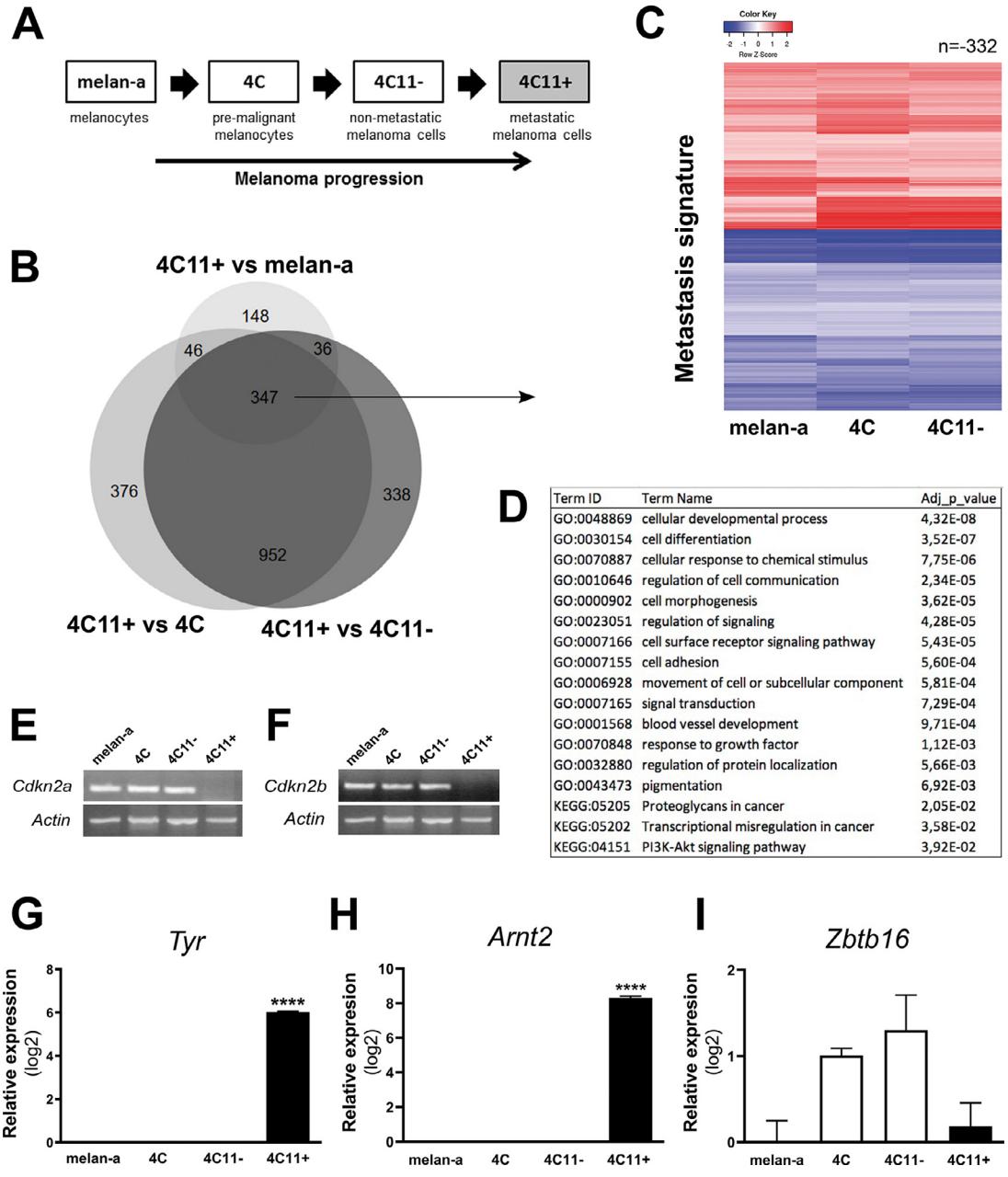

Fig. 3. Identification of a melanoma metastasis signature. (**A**) Progression model schema from nonmalignant melanocytes, premalignant and nonmetastatic (in white) to metastatic melanoma cells (in gray). (**B**) Venn diagram with DEGs in pairwise comparisons between nonmalignant melan-a melanocytes, premalignant 4C and nonmetastatic 4C11- to metastatic 4C11+ melanoma cell lines (log2 ratio $\geq |2|$ and Benjamini-Hochberg adjusted *P*-value ≤ 0.01). (**C**) Heatmap with z-score normalized expression values of 332 DEGs detected in metastatic cells compared to nonmetastatic, premalignant and nonmalignant cells lines (upregulated genes in red, downregulated genes in blue). (**D**) Enriched biological processes and molecular pathways categories in the 332-gene metastasis signature. (**E-F**) Relative expression levels of *Cdkn2a* and *Cdkn2b*, respectively, determined by semiquantitative RT-PCR. (**G-I**) Relative expression levels of *Tyr, Arnt2* and *Zbtb16*, respectively, by RT-qPCR.

an increased expression of markers associated with the undifferentiated, undifferentiated-neural crest-like and neural crest-like categories. In contrast, the differentiated melan-a and 4C11+ cells had an increased expression of markers associated with the neural crest-like-transitory, transitory, transitory-melanocytic and melanocytic subgroups. A significant proportion of these markers was statistically differentially expressed in at least one of the cell lines; out of 315 mapped genes, there were 232, 260, 248 and 252 DE markers ($P_{adj} < 0.01$) respectively in the melan-a, 4C, 4C11- and 4C11+ cells when compared to the other 3 cell lines. Most of these genes ($n = 174$) were commonly DE across all cell lines from our model (Fig. 5**B**). The hierarchical clustering analysis based on the average expression values of these commonly regulated markers has also clustered the cell lines based on their differentiated or "mesenchymal-like" phenotype (Fig. 5**D**).

The cross-reference of DE markers with DEGs between each transition in the melanoma progression model (4C *versus* melan-a, 4C11- *versus* 4C or 4C11+ *versus* 4C11-; Fig. 1**D**), or between the differentiated versus

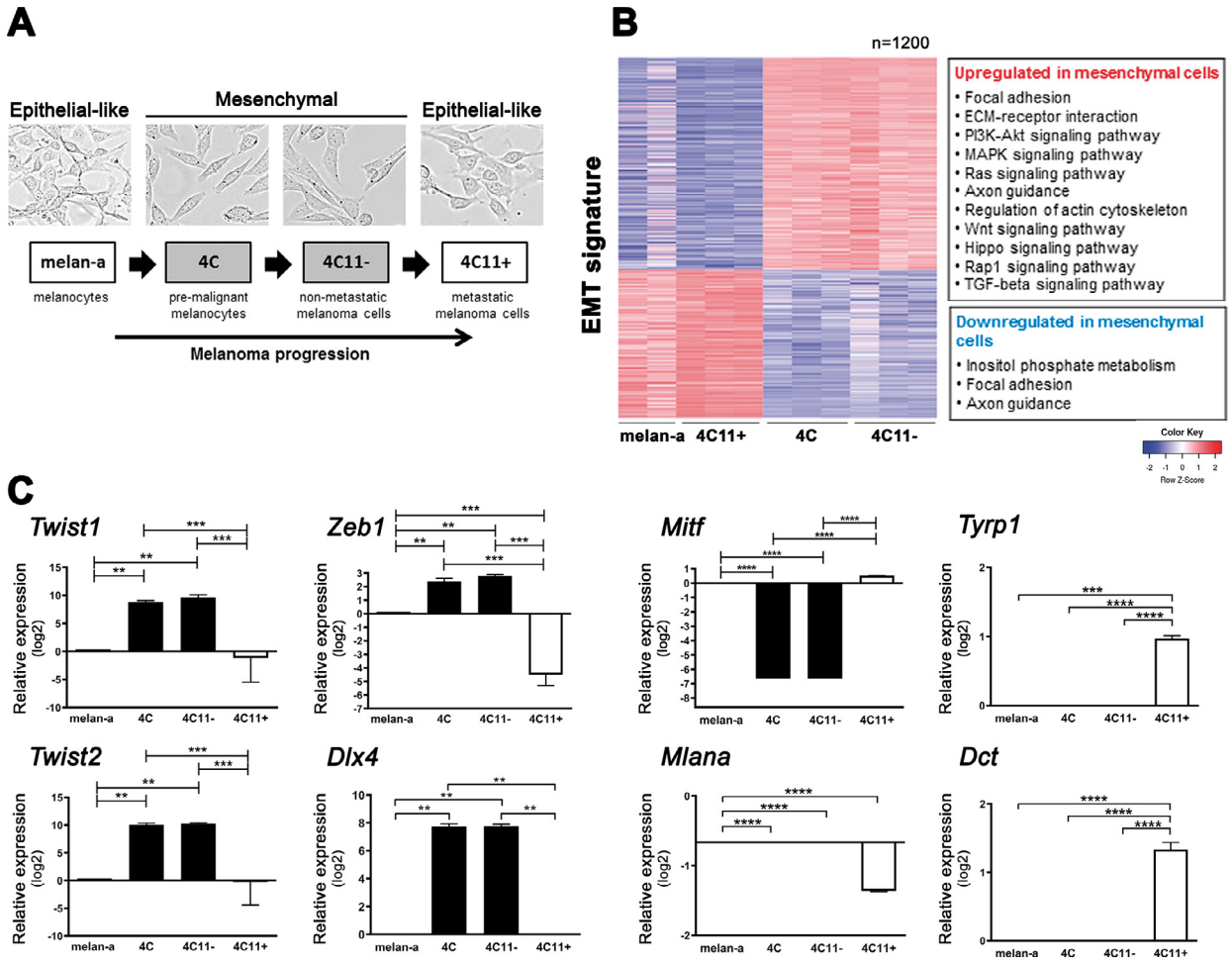

Fig. 4. An EMT gene expression signature associated with melanoma progression. (**A**) The progression model encompasses cell lines with "epithelial-like" (in white) and "mesenchymal-like" (in gray) morphologies. (**B**) Heatmap with 1200 DEGs (log2 ratios $\geq |2|$ and Benjamini-Hochberg adjusted *P*-value $\leq$ 0.01) between cells with epithelial-like (melan-a and 4C11+) or mesenchymal (4C and 4C11-) morphology (upregulated genes in red, downregulated genes in blue). Significantly enriched molecular pathways ($P \leq 0.05$) among genes upregulated or downregulated in cell lines with mesenchymal morphology. (**C**) RT-qPCR validation of genes upregulated (*Twist1, Twist2, Zeb1* and *Dlx4*) and downregulated (*Mitf, Mlana, Tyrp1* and *Dct*) in EMT (see Methods for details).

"mesenchymal-like" cell lines (melan-a and 4C11+ *versus* 4C and 4C11-; **Fig. 4B**), revealed respectively 182, 34, 196 and 226 DE markers (**Fig. 5C**). A higher number of deregulated differentiation markers was identified between the stages when there is phenotypic plasticity. During these transitions, there was a more frequent upregulation (4C *versus* melan-a) followed by reversible downregulation (4C11+ *versus* 4C11-) of DE markers from the undifferentiated and neural crest-like states. Accordingly, a higher number of markers from the transitory and melanocytic human melanoma subtypes were found downregulated during the transition from melanocytes to premalignant 4C cells (**Fig. 5F**) and then reversibly upregulated in the transition from 4C11- to 4C11+ cells (**Fig. 5G**). A similar pattern was observed in the analysis using the EMT signature, in which melanocytic/transitory and neural crest/undifferentiated DE markers were predominantly upregulated in differentiated and "mesenchymal-like" cell lines, respectively (**Fig. 5H**). The functional enrichment of the DE markers in our model has revealed that markers from the undifferentiated and neural crest-like categories are involved in PI3K and MAPK pathways, desmosome assembly, cell-substrate adhesion, extracellular matrix organization, cell migration, and angiogenesis. Conversely, DE markers from the transitory and melanocytic categories were associated with melanin biosynthesis, pigment cell differentiation and regulation of immune response (**Fig. 5E**).

Prognostic value of murine melanoma DEGs in human melanoma

We next investigated the potential of DEGs in our murine melanoma cell model to predict the outcome of melanoma patients. First, we compiled a list of 2349 unique DEGs detected in all pairwise comparisons between cell lines (**Fig. 1D**, **Fig. S1**), which included those present in the malignancy (**Fig. 2C**), metastasis (**Fig. 3C**), and EMT (**Fig. 4B**) signatures. These genes were then mapped to their human gene orthologs, retrieving a total of 2093 genes. Using data from the Leeds Melanoma Cohort (treatment naïve, primary melanoma, n=703, median follow up=8 y), we have found that the expression levels of 766 genes were significantly associated with patient outcome (Cox's regression $P \leq 0.05$), consistent with the changes detected in the murine cellular model (**Table S8**). Of note, most genes (607 out 766, 79%) remained significantly associated with patient outcome after adjusting for the clinical covariables age, sex, site, AJCC stage and mitotic rate. These comprised 11 genes from the malignancy signature (including *Timp1,* HR 1.4, 95%CI 1.02–1.9; and *Nqo1,* HR 1.4, 95%CI 1.0–1.9), 43 genes from the metastasis signature (including *Zbtb16,* HR 0.7; 95%CI 0.5–1.0; and *Arnt2,* HR 1.5; 95%CI 1.1–2.0) that showed independent association with patient survival after adjusting for clinical covariates (**TABLE 1** and **2,** respectively), as well as 301 genes from the EMT signature (including *Mitf,* HR 1.3; 95%CI 1.0–1.8; and

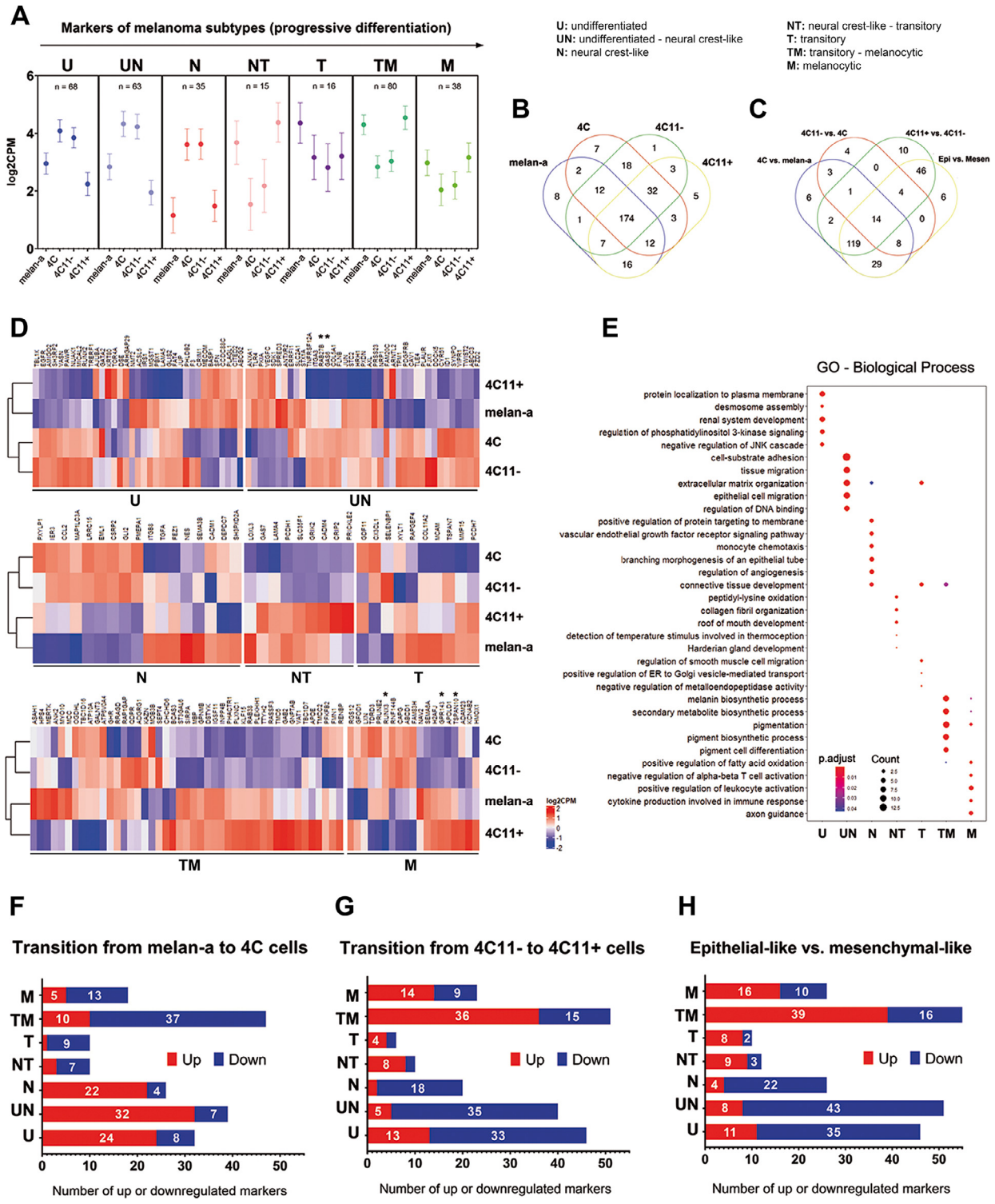

Fig. 5. Expression of markers from the human melanoma differentiation trajectory across the cell lines from the linear model of melanoma progression. Tsoi et al. (2018) identified gene markers whose expression levels were deregulated in one of 4 progressive stages of melanoma differentiation (undifferentiated, neural crest-like, transitory and melanocytic), or exhibited common differential expression between 2 adjacent subtypes (undifferentiated-neural crest-like, neural crest-like-transitory and transitory-melanocytic). (**A**) The expression profile of murine orthologs from these DE markers was analyzed in our model to determine the extent each cell line could be related with a phenotypic state in the human melanoma differentiation trajectory. Mesenchymal-like cell lines (4C and 4C11-) showed an increased expression of markers associated with the undifferentiated (U), undifferentiated-neural crest-like (UN) and neural crest-like categories (N), whereas epithelial-like cells (melan and 4C11+) showed a higher expression of markers from the neural crest-like-transitory (NT), transitory (T) and melanocytic (M) categories. (**B**) Venn diagram analysis showing the overlap among DE markers detected in each cell line. (**C**) Murine orthologs from human melanoma DE marker were cross-referenced with DEGs detected along each transition stage of the melanoma progression (from Fig. 1D), or between epithelial-like and mesenchymal-like cells (from Fig. 4B) and Venn diagram shows the overlap among DE markers detected in each pairwise comparison. A higher number of DE markers was observed in the transitions in which cellular morphology was changed. (**D**) The 174 DE markers detected in all cell lines (upregulated genes in red, downregulated genes in blue) were used to perform a hierarchical clustering analysis, which have grouped the cell lines according to their epithelial or mesenchymal-like morphologies. Asterisks (*) indicate genes with prognostic value as shown in Tables 1 and 2. (**E**) Functional enrichment

Table 1

Prognostic and biological significance of the melanoma malignancy signature.

Gene Symbol	Expression (Murine Model)	Human Ortholog	Hazard Ratio(95% CI)	Adj. *P* value	Description	Association With Cancer			Remarks
						Bio	Mel	Can	
Itga8	down	***ITGA8***	**0.612** (0.461–0.814)	<0.001	Integrin subunit alpha 8	-	-	12	Low expression as independent predictive factor of overall survival of clear cell renal cell carcinoma[1], and prognostic factor in colorectal carcinogenesis[2]
Nr3c2	down	***NR3C2***	**0.759** (0.573–1.004)	0.050	Nuclear receptor subfamily 3 group C member 2	-	-	27	Low expression as a poor prognosis in colon[3], hepatocellular[4], renal cell[5,6], and prostrate carcinomas[7,8].
Cacng7	up	***CACNG7***	**1.974** (1.436–2.713)*	<0.001	Calcium channel, voltage-dependent, gamma subunit 7	-	-	3	Expressed in some types of stem cells[9,10]; Epigenetic regulation[9,11]
Nqo1	up	***NQO1***	**1.400** (1.025–1.909)*	0.034	NAD(P)H quinone dehydrogenase 1	√	33	1443	Oncogenic role in melanoma[12,13]; High expression correlates with poor melanoma patient outcome[14,15]
Timp1	up	***TIMP1***	**1.387** (1.016–1.891)*	0.039	Tissue inhibitor of metallopeptidase 1	√	26	728	High expression as a poor prognosis in melanoma[16-20]
Fkbp10	up	***FKBP10***	**1.373** (1.007–1.871)*	0.044	FKBP prolyl isomerase 10	-	1	17	Expression induced by HRAS[21]; Oncogenic role in gastric cancer[22] and renal cell carcinoma[23]
Chst10	up	***CHST10***	**1.504** (1.134–1.993)	0.004	Carbohydrate sulfotransferase 10	-	2	8	Regulated by RARgamma in a subset of human melanoma cells[24]
Sall4	up	***SALL4***	**1.444** (1.089–1.913)	0.010	Spalt like transcription factor 4	-	3	341	Expressed in cancer stem cells subpopulation in melanoma metastasis in the brain[25]
Fstl1	up	***FSTL1***	**1.347** (1.019–1.781)	0.036	Follistatin like 1	-	1	52	Promotes bone metastasis and immune dysfunction in melanoma patients[26]
Trim71	up	***TRIM71***	**1.328** (1.004–1.755)	0.046	E3 ubiquitin ligase tripartite motif containing 71	-	-	10	Critical regulator of stem cell fates that antagonizes p53-dependent pro-apoptotic and pro-differentiation responses[27]; Promotes proliferation of nonsmall cell lung cancer[28]
Hoxa10	up	***HOXA10***	**1.338** (1.010–1.773)	0.042	Homeobox A10	-	1	246	Oncogenic role in different types of cancer, such as AML[29], and ovarian[30], lung[31], hepatocellular carcinomas[32]

Genes down or upregulated in the malignancy signature of the murine melanoma model, and with orthologs identified as independent prognostic markers for melanoma patients (see Methods for details). Estimated hazard ratios (HR) were adjusted for age, sex, anatomical site, or these previous variables plus AJCC stage and mitotic rate (indicated by asterisk). Cox's regression HR is shown along 95% confidence interval and adjusted *P*-values (Leeds melanoma cohort). Cited references listed in the supplementary material. Bio: melanoma biomarker; Mel: number of studies reported in melanoma; Can: number of studies reported in cancer (March 2020).

Table 2

Prognostic and biological significance of melanoma metastasis signature.

Gene Symbol	Expression (Murine Model)	Human Ortholog	Hazard Ratio (95% CI)	Adj.*P* Value	Description	Association With Cancer			Remarks
						Bio	Mel	Can	
Gas6	down	***GAS6***	**0.645** (0.465–0.895) *	0.009	Growth arrest specific 6	-	15	274	Correlation between Gas6 and Axl expression seems to be related to melanocyte development and pigmentation, invasion, and microenvironment interactions[33]
Pck2	down	***PCK2***	**0.676** (0.495–0.921) *	0.013	Phosphoenolpyruvate carboxykinase 2, mitochondrial	-	1	44	Downregulated in tumor-repopulating cells of melanoma, favoring their growth and tumorigenesis[34]
Anxa6	down	***ANXA6***	**0.681** (0.497–0.933) *	0.017	Annexin A6	-	1	38	Tumor suppressor function in different types of cancer, including melanomas[35,36]
Runx3	down	***RUNX3***	**0.684** (0.500–0.933) *	0.017	RUNX family transcription factor 3	√	13	857	Reduced expression correlated with poor survival in melanoma patients[37]
Pdgfb	down	***PDGFB***	**0.688** (0.499–0.948) *	0.022	Platelet derived growth factor subunit B	-	48	1280	Melanoma cells expressing PDGF-B without its retention motif have more myeloid-derived suppressor cells, that inhibit T-cell–mediated antitumor immunity[38]
Zbtb16	down	***ZBTB16***	**0.695** (0.506–0.954) *	0.024	Zinc finger and BTB domain containing 16	√	12	200	Low expression in melanoma cells compared to melanocytes, associated with tumorigenic phenotype and a less differentiated state[39]; Expression in primary malignant melanoma patients as a predictor of long-term survival[40]
Nkd2	down	***NKD2***	**0.709** (0.509–0.988) *	0.043	NKD inhibitor of WNT signaling pathway 2	-	-	37	Low expression associated with poor prognosis in hepatocellular carcinoma[41] and AML[42]; Induces switch from the WNT/GSK3beta to the WNT/PCP signaling pathway[43]
Vdr	down	***VDR***	**0.735** (0.537–1.005) *	0.053	Vitamin D receptor	√	102	1880	Vitamin D / VDR signaling contributes to control pro-proliferative[44] / immunosuppressive Wnt/β-catenin signaling in melanoma[45]
Tiam2	down	***TIAM2***	**0.736** (0.536–1.009) *	0.056	TIAM Rac1 associated GEF 2	-	-	16	Downregulation decreases nuclear stiffness and reduces expression of TAZ-regulated genes[46]
Ahnak	down	***AHNAK***	**0.577** (0.432–0.770)	<0.001	AHNAK nucleoprotein	√	4	69	Seems to be required for the expression of functional E-cadherin; Downregulation predicts poor outcome in melanoma[47]
Rab27b	down	***RAB27B***	**0.601** (0.446–0.807)	<0.001	RAB27B, member RAS oncogene family	-	2	49	Downregulated in advanced prostate cancer[48]; Low expression as a poor prognosis in colorectal cancer[49]
Krt10	down	***KRT10***	**0.619** (0.459–0.825)	0.001	Keratin 10	-	2	71	Described as a negative modulator of cell cycle progression[50]
Maf	down	***MAF***	**0.620** (0.462–0.831)	0.001	MAF bZIP transcription factor	-	-	30	Activator of the transcription factor Nrf2, involved in antioxidant and pro-apoptotic response[51]; A novel transcriptional target of Hh signaling that control cell-cell adhesion by negative regulation of E-cadherin expression in Drosophila[52,53]
Ank3	down	***ANK3***	**0.627** (0.468–0.840)	0.002	Ankyrin 3	-	2	309	Downregulation during oncogenic EMT suppresses p14ARF and confers *anoikis* resistance in melanoma[54]

(*continued on next page*)

Table 2 (*continued*)

Gene Symbol	Expression (Murine Model)	Human Ortholog	Hazard Ratio (95% CI)	Adj.*P* Value	Description	Association With Cancer			Remarks
						Bio	Mel	Can	
Gsn	down	***GSN***	**0.662** (0.497–0.880)	0.005	Gelsolin	-	1	87	Identified as enhanced in metastatic exosomes in melanoma[55]
Fgfr2	down	***FGFR2***	**0.675** (0.505–0.902)	0.008	Fibroblast growth factor receptor 2	-	25	1316	Loss-of-function mutations described in melanomas[56]
Fam107b	down	***FAM107B***	**0.694** (0.524–0.920)	0.011	Family with sequence similarity 107 member B	-	-	4	Downregulated in gastric, colorectal, colon, breast, thyroid, testis and uterine cervix cancer[57-58]
Casp1	down	***CASP1***	**0.718** (0.543–0.950)	0.020	Caspase 1	-	1	114	Low expression correlated with poor overall survival in lung adenocarcinoma[59]
Scara5	down	***SCARA5***	**0.724** (0.546–0.960)	0.025	Scavenger receptor class A member 5	-	-	24	Tumor suppressor in thyroid[60], breast[61], renal cell[62] and hepatocellular carcinoma[63]
Tagln2	down	***TAGLN2***	**0.727** (0.549–0.962)	0.026	Transgelin 2	-	-	40	Downregulation promotes breast cancer metastasis[64]; Overexpression inhibits cervical cancer cell invasion and migration[65]
Klf4	down	***KLF4***	**0.732** (0.550–0.973)	0.032	Kruppel like factor 4	-	30	1142	Downregulated in melanoma cell lines with homozygous deletion of the CDKN2A gene[66]
Ksr1	down	***KSR1***	**0.734** (0.555–0.969)	0.029	Kinase suppressor of ras 1	-	4	80	The loss of its interaction with BRAF leads to the attenuation of the MEK-ERK signaling[67]
Plp2	down	***PLP2***	**0.737** (0.556–0.975)	0.033	Proteolipid protein 2	-	3	9	Enhances proliferation, adhesion, invasion in murine melanoma cells[68]
Fam180a	down	***FAM180A***	**0.740** (0.557–0.982)	0.037	Family with sequence similarity 180 member A	-	-	-	-
Ptprf	down	***PTPRF***	**0.742** (0.559–0.985)	0.039	Protein tyrosine phosphatase receptor type F	-	2	46	Upregulation inhibits breast cancer progression[69]; Tumor suppressor in gastric[70] and colorectal cancer[71]
Gas1	down	***GAS1***	**0.745** (0.563–0.986)	0.040	Growth arrest specific 1	-	3	88	Metastasis suppressor in melanoma[72]
Arhgap22	down	***ARHGAP22***	**0.753** (0.569–0.996)	0.047	Rho GTPase activating protein 22	-	5	9	Epigenetic silencing contributes to invasion of primary tumors and invasion-related melanoma progression[73,74]
Pou4f1	up	***POU4F1***	**1.510** (1.103–2.066) *	0.010	POU class 4 homeobox 1, BRN3A	-	2	44	Expressed in melanoma and required for cell cycle progression and survival[75]
Taf9b	up	***TAF9B***	**1.504** (1.097–2.063) *	0.011	TATA-box binding protein associated factor 9b	-	-	4	Essential for cell growth in human cells[76]
Arnt2	up	***ARNT2***	**1.485** (1.085–2.031) *	0.013	Aryl hydrocarbon receptor nuclear translocator 2	-	1	29	Binds and has its transcriptional activity positively regulated by MAGE1[77]; Key transcription factor controlling glioblastoma cell aggressiveness[78]; Role in tumor angiogenesis and the neural response to hypoxia[79]
Zfp532	up	***ZNF532***	**1.440** (1.054–1.968) *	0.022	Zinc finger protein 532	-	-	7	LncRNA; Increased expression in drug-resistant pancreatic cancer[80]; Regulates the oncogenic chromatin complex in BRD4-NUT patient cells[81]
Tubg2	up	***TUBG2***	**1.423** (1.042–1.942) *	0.026	Tubulin gamma 2	-	-	7	Increased expression in lung cancer[82], and neuroblastoma cells[83]

(*continued on next page*)

Table 2 (*continued*)

Gene Symbol	Expression (Murine Model)	Human Ortholog	Hazard Ratio (95% CI)	Adj.*P* Value	Description	Association With Cancer			Remarks
						Bio	Mel	Can	
Cmtm5	up	***CMTM5***	**1.383** (1.013–1.886) *	0.041	CKLF like MARVEL transmembrane domain containing 5	-	-	23	Suppressor effects in cervical[84], pancreatic[85], ovarian[86] and renal[87] carcinomas
Gpr143	up	***GPR143***	**1.353** (0.987–1.855) *	0.059	G protein-coupled receptor 143	-	14	16	Induces melanoma cell migration mediated through the RAS/RAF/MEK/ERK signaling pathway[88]; Role in melanosome biogenesis and activation of MITF expression[89]; Associated with chemoresistance[90]
Gbe1	up	***GBE1***	**1.475** (1.116–1.949)	0.006	1,4-alpha-glucan branching enzyme 1	-	1	11	Expression correlates with the lack of response of melanoma patients to immunotherapy[91]
Slc25a13	up	***SLC25A13***	**1.424** (1.075–1.887)	0.014	Solute carrier family 25 member 13	-	-	10	Expression associated with tumor aggressiveness, metabolic adaptation to nutritional stress, and poorer prognosis of colorectal cancer[92]
Neto2	up	***NETO2***	**1.422** (1.073–1.883)	0.014	Neuropilin and tolloid like 2	-	1	16	Overexpressed and presenting oncogenic effects in colorectal[93], prostate[94], gastric[95], and nasopharyngeal[96] carcinomas
Gja3	up	***GJA3***	**1.410** (1.064–1.867)	0.017	Gap junction protein alpha 3	-	1	10	Role in the maintenance of glioblastoma CSC[97]
Fam178b	up	***FAM178B***	**1.398** (1.053–1.857)	0.020	FAM178B family with sequence similarity 178 member B	-	-	-	-
Ccng1	up	***CCNG1***	**1.383** (1.045–1.828)	0.023	Cyclin G1	-	1	194	Growth-promoting function through activation of MDM2 oncogene; Overexpressed in osteosarcomas, breast, prostate, colorectal and HCC cancers, and is correlated with a poor prognosis[98]
Tspan10	up	***TSPAN10***	**1.353** (1.021–1.793)	0.035	Tetraspanin 10	-	2	6	Downregulation reduces melanoma cell migration[99]
Insc	up	***INSC***	**1.350** (1.022–1.781)	0.034	INSC spindle orientation adaptor protein	-	-	16	Role in asymmetric divisions of mammary stem cells[100]; Associates with Hippo pathway downstream kinases[101]
Fstl1	up	***FSTL1***	**1.347** (1.019–1.781)	0.036	Follistatin like 1	-	2	52	Induces bone metastasis and antitumor immunity in melanoma[102]

Genes found as down or upregulated in the metastatic signature of murine melanoma model, and with orthologs identified as independent prognostic markers for survival in melanoma patients are shown (see Methods for details). Hazard ratios (HR) were adjusted for age, sex, anatomical site, or these previous variables plus AJCC stage and mitotic rate (indicated by asterisk). Cox's regression HR is shown along 95% confidence interval and adjusted *P*-values (Leeds melanoma cohort). Cited references listed in the supplementary material. Bio: melanoma biomarker; Mel: number of studies reported in melanoma; Can: number of studies reported in cancer (searched in March 2020). *References available in supplementary information.

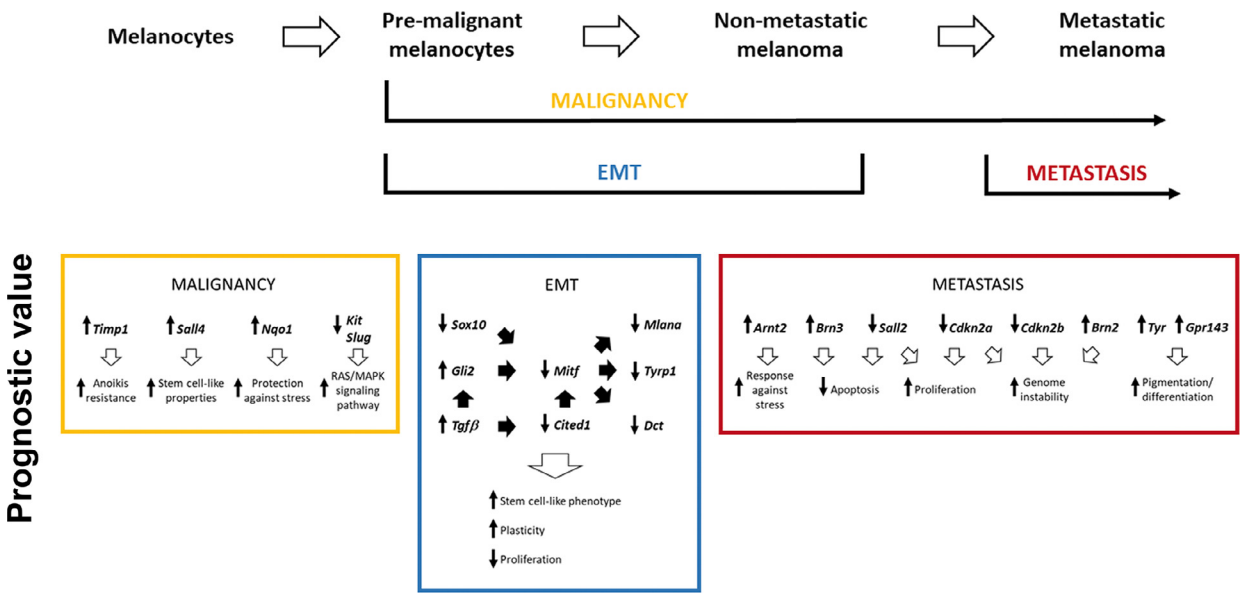

Fig. 6. Transcriptional signatures in the murine melanoma progression model comprise genes sustaining malignant phenotypes that are associated with patient outcome. Selected genes in the malignancy, metastasis and EMT signatures identified as independent prognostic factors and the cellular processes affected by their deregulation are shown during melanoma progression.

Dlx4, HR 1.4; 95%CI 1.1–1.9). A summary of the key genes contained in the malignancy, metastasis and EMT signatures and identified as independent prognostic factors, and the cellular processes affected by their deregulation during melanoma progression, is shown in **Figure 6**.

Discussion

In the present work, we have investigated the transcriptional events involved in early and late stages of melanoma progression, as well as in cell plasticity, to shed light on novel biomarkers and drug targets for this disease. The comparative analysis of the transcriptome profiles in the cell lines from our 4-stage murine model revealed dynamic transcriptional changes that take place during melanoma initiation and progression. Of note, early steps of tumor progression (4C and 4C11- cells) were characterized by gene expression signatures consistent with EMT and acquisition of stem cell-like phenotypes, whereas the differential transcriptome of the metastatic cell line (4C11+) was characterized by the alteration of genes associated with highly proliferative and differentiated cells, as described by Hoek and Goding for human melanomas [30]. In addition, we have matched the transcriptional patterns of each cell line with markers that characterize different stages of human melanoma differentiation, as described by Tsoi and colleagues [9]. This analysis revealed that the differentiated cell lines (melan-a and 4C11+) in our model have increased expression of transitory and melanocytic markers, whereas the mesenchymal-like cells (4C and 4C11-) show the upregulation of markers from the undifferentiated and neural crest-like states. These results indicate that the murine progression model recapitulates phenotypic and molecular changes observed in human melanoma. Other recent studies based on single-cell RNA sequencing (scRNAseq) corroborate the existence of different transcriptional states during melanoma evolution that contribute to intratumor cellular heterogeneity and have impact on disease outcome. Using an elegant melanoma patient-derived xenograft (PDX) model of minimum residual disease (MRD), Rambow and colleagues (2018) have described 4 distinct cell states – pigmented, invasive, neural crest stem cells, and starved melanoma cells, in drug-tolerant $BRAF^{V600E}$ melanoma cells. Similarly, by using a transgenic zebrafish melanoma model that expresses human $BRAF^{V600E}$, in P53 null background, Baron et al (2020) have found 3 transcriptional states after analyzing melanoma single cells – neural crest, mature melanocytes and stress-like, being the first and the last induced in drug-resistant cells. Cycling ($MITF^{high}$) and noncycling ($MITF^{low}$) melanoma cell subpopulations were identified by Tirosh et al (2016) after sequencing single cells from 19 metastatic melanoma samples, including both tumors with mutations in BRAF and NRAS, and wild-type BRAF/NRAS.

Although the transcriptional programs identified in our cell lines converge with those described by these previous studies using patient-derived bulk tissue and cell lines or animal genetic models, the findings from our model are novel since i) the transcriptional signatures were identified using a sequential model that recapitulates the time course of melanoma progression using cell lines having a similar genetic background, and ii) no drug treatment was applied as a selective pressure to generate drug-resistant cells. Also, unlike most studies that evaluated intratumoral heterogeneity in $BRAF^{V600E}$ melanomas, our stepwise cell model does not present mutations in melanoma driver genes, such as *Braf, Nras* and *Rac1,* or in *Mitf* and *Trp53* (data not shown). Curiously, despite no mutation was found in these genes, they are all abnormally activated or expressed along our melanoma progression model (Molognoni et al., 2013), which points to the existence of dynamic regulatory molecular mechanisms. In fact, in our model, epigenetic mechanisms were involved in the melanocyte malignant transformation induced by sequential cycles of de-adhesion/adhesion (Campos et al., 2007; Molognoni et al., 2011; Souza et al., 2012; Molognoni et al., 2013; Azevedo et al, 2020). Melanoma cell plasticity is a common resistance mechanism to clinically available immunotherapies and kinase inhibitors targeting cell proliferation. Consequently, our linear model of melanoma progression may be used to screen novel therapeutic strategies with translational validity to target dedifferentiated melanoma cell subtypes, which are marked by a low proliferation phenotype and the masking of immune epitopes. Moreover, given their murine origin, the tumorigenic cell lines from our model could be employed to screen drugs *in vivo* in immunocompetent mice, especially the metastasis-prone 4C11+ cells that may recapitulate EMT in vivo during metastasis.

The DEGs between cell lines with increasing malignancy along tumor progression included many genes involved in pluripotency, and were

enriched for signaling pathways, such as Hippo and WNT, during the transition between melanocytes and premalignant melanocytes. The direction of the expression changes of the genes from these pathways was inverted during the transition between slow-growing and nonmetastatic 4C11- to fast-growing and metastatic 4C11+ melanoma cells. Likewise, a reduced expression of genes involved in melanogenesis was noted in the melan-a to 4C transition and was reverted in the 4C11- to 4C11+ transition. The dynamic switching between differentiated/proliferative and mesenchymal/slow-cycling phenotypes is an important phenomenon in human melanoma accounting for tumor heterogeneity and drug resistance [31-33]. Accordingly, our study contributes to a better understanding of the dynamics in gene expression changes underlying cell plasticity during melanoma progression.

Three different transcriptional signatures were recognized across the cell lines as associated with malignancy, metastasis and EMT. These signatures contain genes that affect biological processes critical to sustain melanoma progression and metastasis, and subsets of these genes were significantly associated with melanoma prognosis. Novel insights derived from the functional annotation of genes in these signatures are discussed below. The malignancy signature was overrepresented by genes involved in embryo development and morphogenesis. For instance, the cancer stem cell marker *Sall4* was upregulated in this signature, in line with its increased expression in tumor subpopulations of melanoma brain metastasis [34]. *Nqo1*, also upregulated in this signature, is overexpressed in human melanomas and mediates detoxification of oxygen radicals and protection against different stress types [35,36]. Of note, our murine melanoma model was established based on a lasting stressful condition - adhesion impediment - which resulted in oxidative stress and malignant transformation [37,38,8]. Since malignant transformation was induced by sustained cellular stress, elevated levels of *Nqo1* might reflect an attempt to maintain cell homeostasis. *Timp1* was also highly expressed from early to late stages of melanoma progression compared to melan-a melanocytes. In addition to its well-known role in matrix metalloproteinases (MMPs) inhibition, TIMP1 can also have oncogenic roles in cancer, as demonstrated by our group and others [39,40]. Finally, in our model, *Kit* was downregulated during malignant progression. *Kit* is a proto-oncogene in mucosal and acral melanomas, but paradoxically, it is barely expressed in cutaneous melanomas occurring on intermittently or chronically sun-damaged skin, which are mainly driven by *BRAF*- or *NRAS*-activating mutations [41]. In a zebrafish $BRAF^{V600E}$ melanoma model, Neiswender and colleagues [42] showed that the loss of *Kit* led to an increased rate of tumor initiation. While *Kit* expression was reduced in all transformed cell lines compared to melan-a, a 5-fold increase was seen in 4C11+ compared to 4C/4C11- cells, suggesting a possible role of *Kit* in melanoma metastasis. We have also found that *Snai2* (*Slug*), a downstream target of KIT activation [43], was downregulated in the malignancy signature, pointing to the attenuation of c-Kit signaling during melanoma progression. Together, the genes from the malignancy signature highlight stress response, *anoikis* resistance, acquisition of stem cell-like features, and RAS/MAPK signaling as early events in melanoma progression.

The metastasis signature identified in the model was enriched with genes involved in cell differentiation, blood vessel development, cell communication and intracellular signaling. The *Tyr* and *Gpr143* genes encode markers of cell differentiation and pigmentation that were highly expressed in 4C11+, whereas several stem cell-related genes (e.g. *Klf4, Sall2, Sox12, Gas1, Gas6, Bmp1* and *Fat4*) were downregulated. These results indicate that the acquisition of metastatic potential in late stages of melanoma progression is associated with the transition to a more differentiated phenotype.

Several genes from the metastasis signature are associated with aggressive tumor phenotypes. For instance, Bogeas and colleagues [44] showed higher expression of ARNT2 in proliferative cell sub-populations in glioblastoma. Moreover, they revealed an association between ARNT2 knockdown and loss of cell tumorigenicity, via the repression of *SOX9, POU3F2* (BRN2) and *OLIG2*. In our model, the metastatic 4C11+ cell line had increased levels of *Arnt2* and higher levels of *Pou3f2* compared to 4C and 4C11- cells. Given that melanomas and glioblastomas have the same neuroectodermal origin, despite possible differences in signaling events, our data suggest that *Arnt2* might have a similar role in promoting cell aggressiveness in melanoma.

Patel and colleagues [45] have demonstrated that the loss of both *Cdkn2a* and *Cdkn2b* contributes to genome instability in late stages of melanoma progression. While the consequences of *CDKN2A* inhibition to melanoma pathogenesis are better known than those of *CDKN2B*, the p15 protein encoded by *CDKN2B* is highly expressed in benign melanocytic nevi, and its loss promotes the transition from benign nevus to melanoma [46]. In agreement with these observations, the expression of both *Cdkn2a* and *Cdkn2b* is lost in the metastatic 4C11+ cells. Moreover, 4C11+ cells have a lower expression of *Sall2*, whose encoded protein suppresses tumorigenesis through cell cycle inhibition and apoptosis induction. Searching for SALL2-responsive genes, Wu and collaborators [47] have identified p16(INK4A), the product of *CDKN2A*, as an important mediator of SALL2-dependent effects on cell cycle. The upregulation of *Brn2* in the metastatic signature suggests that increased genome instability might be found in metastatic 4C11+ cells. Indeed, we have previously detected centrosome fusions and significant chromosomal instability in cell lines corresponding to the late stage of melanoma progression [48,7]. Recently, a high somatic mutation burden in melanoma was also associated with BRN2 expression, which also suppresses apoptosis and promotes error-prone DNA damage repair [49]. In parallel, *Zbtb16* (Plzf) has tumor suppressor functions in different cancers, including melanoma [50,51], which is in line with its lower expression in the metastasis-prone 4C11+ cells. Other genes previously associated with tumor aggressiveness were also identified in the metastasis signature, such as *Pou4f2* (Brn3), *Mgat5, Cdkn1a* (p21), *Mapk12, Mdm2*, and *Ngfr* (upregulated), and *Vdr, Lef1, Axl, Fzd8, Fat4, Shroom3, Igfbp2, Ksr1* and *Pck2* (downregulated), which may contribute to the aggressive phenotype of 4C11+ cells. Collectively, the differential transcriptome profile of metastatic 4C11+ cells indicates that these cells phenocopy the pigmented, differentiated and proliferative phenotype recognized in human melanoma [28].

Genes from the EMT signature were enriched for biological pathways involved in ECM-receptor interaction, TGF-beta, Wnt and Hippo pathways. Among the upregulated genes in this signature, we have identified the classical EMT markers *Snai1, Twist1, Twist2, Zeb1* and *Bgn*. Moreover, the mesenchymal cell lines had increased expression of *Tgfβ3* and a depletion of *Mitf* and MITF downstream targets (*Mlana, Tyrp1* and *Dct*). TGFβ is a well-known EMT inducer that generates quiescent stem cells and promotes MITF downregulation in melanoma [52]. CITED1, a MITF regulator previously shown to be repressed by TGFβ [53], was also downregulated in the EMT signature. In the original study, CITED1 was associated with a proliferative state and recognized as a molecular driver of melanoma phenotype switching. SOX10 also plays a role in controlling MITF expression, via promoter binding and transcriptional upregulation [54]. SOX10 is highly expressed in melanomas, and is expressed at low levels in "mesenchymal-like" cells and highly expressed in the "epithelial-like" metastatic 4C11+ cells, showing the same pattern of *Mitf*. MITF, the master regulator of melanocytic differentiation, is a central hub in the control of the transition between different phenotypic states [30]. MITF-depleted cells show a stem cell-like phenotype, increased plasticity, and reduced proliferation, whereas MITF-high cells have a proliferative and differentiated phenotype. This pattern was also observed in our model: the EMT signature was enriched with several stem cell-related genes, such as *Sox9, Gli1, Gli2, Cd24a, Klf5, Igf1, Gas1, Gas6, Bmp4, Gfra1, Arid3b, Ror1, Notch3, Dlx5*, and *Dlx4*. The transcription factor GLI2, acting downstream in the Hedgehog signaling pathway and regulated by TGFβ, is able to repress MITF [55]. These results highlight the cell plasticity occurring during melanoma progression, supporting that

melan-a cells undergo EMT during malignant transformation, which could be somewhat reversed upon acquisition of metastatic features in 4C11+ cells.

To confirm the validity of our model in detecting clinically relevant targets, the prognostic value of DEGs was investigated using expression and clinical data from the Leeds Melanoma Cohort. In the malignancy signature, 11 genes were identified as independent prognostic factors. Seven out 11 of these genes have already been described in melanomas, and are related to stress response, apoptosis resistance and stem cell-like phenotype. In the metastasis signature, 43 genes were found as prognostic factors for melanoma patients. Twenty out of the 27 downregulated genes have been previously reported in melanomas, and 4 of them (*Runx3, Zbtb16, Vdr* and *Ahnak*) had lower expression associated with poor prognosis. Nine out of the 16 upregulated genes in the metastasis signature have been described in melanoma, but none as a prognostic biomarker. The genes with prognostic value in the metastatic signature were related to cell differentiation, proliferation, drug resistance, invasion, cell signaling and metastasis. Among those, the expression of *RAB27B, GAS6* (undifferentiated/ neural crest-like markers) and *RUNX3* (a melanocytic marker) - downregulated in 4C11+ (**Fig. 5D**) - correlated with good survival; whereas the expression of the melanocytic markers *GPR143* and *TSPAN10* was highly expressed in 4C11+ cells and correlated with poor survival. Finally, the expression of 302 genes from the EMT signature (102 up and 200 downregulated) also afforded prognostic information about melanoma patients. Genes in the EMT signature implicated with poor survival were related to cell differentiation, angiogenesis and proliferation, whereas those correlated to good prognosis participate in apoptosis and immune response. Indeed, the dedifferentiation of melanoma cells can lead to resistance to immune therapies, since it provides a mechanism to evade immune recognition [9].

Taken together, these findings highlight the translational value of our 4-stage cellular model of melanoma progression as a system to investigate different phenotypes existing in melanoma cells, both *in vitro* and *in vivo*, and to understand molecular mechanisms regulating cell plasticity, which may bring to light novel therapeutic targets. This model is also unique since it represents a linear, progressive model of melanoma, where cell lines have the same genetic background, and can be employed *in vivo* to evaluate biological changes in melanoma in an immunocompetent environment.

Significance

The present study provides evidence that this stepwise cellular model of melanoma progression, developed based on a sustained cellular stress condition (forced anchorage impediment), is a suitable system i) to investigate molecular changes underlying melanocyte malignant transformation and acquisition of aggressive phenotypes, including those related to cell plasticity, melanoma heterogeneity, and drug resistance, as well as ii) to identify potential clinically-relevant prognostic markers of the disease, supported by results obtained using human melanoma transcriptome data.

Credit author statement

Diogo de Oliveira Pessoa: Methodology, Software, Investigation, Data Curation, Writing - Original Draft; Flávia Eichemberger Rius: Methodology, Software, Investigation, Data Curation; Debora D'Angelo Papaiz: Methodology, Validation; Ana Luísa Pedroso Ayub: Methodology, Validation; Alice Santana Morais: Methodology, Validation; Camila Ferreira de Souza: Methodology, Validation; Vinicius Ferreira da Paixão: Methodology; João Carlos Setubal: Formal analysis; Julia Newton-Bishop: Resources; Jérémie Nsengimana: Formal analysis; Hatylas Azevedo: Methodology, Software, Investigation, Data Curation, Writing - Review & Editing, Visualization; Eduardo Moraes Reis: Conceptualization, Methodology, Resources, Data Curation, Writing - Review & Editing, Supervision; Miriam Galvonas Jasiulionis: Conceptualization, Methodology, Resources, Writing - Original Draft, Writing - Review & Editing, Visualization, Supervision, Project administration, Funding acquisition.

Availability of supporting data

The RNA-seq data are accessible through the Gene Expression Omnibus (https://www.ncbi.nlm.nih.gov/geo/) under the accession number GSE149884.

Funding sources

This work was supported by the São Paulo Research Foundation/FAPESP grants # 2018/20775-0 and # 2014/13663-0 (MGJ), # 2009/51462-9 (CFS), # 2011/18959-7 and # 2014/01168-5 (ASM), and # 2017/25321-5 and # 2019/05641-0 (ALPA), by the Conselho Nacional de Desenvolvimento Científico e Tecnológico / CNPq # 140594/2014-0 (FER), and by Coordenação de Aperfeiçoamento de Pessoal de Nível Superior/CAPES # 88882.330516/2019-01 (DAP). MGJ and EMR receive established researcher fellowships from CNPq.

Declaration of competing interest

The authors declare that they have no competing interests.

References

1 Hachey SJ, Boiko AD. Therapeutic implications of melanoma heterogeneity. *Exp. Dermatol.* 2016;**25**:497–500.

2 Palmieri G, Colombino M, Casula M, Manca A, Mandalà M, Cossu AItalian Melanoma Intergroup (IMI). Molecular pathways in melanomagenesis: what we learned from next-generation sequencing approaches. *Curr. Oncol. Rep.* 2018;**20**(11):86.

3 Shain AH, Joseph NM, Yu R, Benhamida J, Liu S, Prow T, et al. Genomic and transcriptomic analysis reveals incremental disruption of key signaling pathways during melanoma evolution. *Cancer Cell* 2018;**34**(1):45–55 e4.

4 Shain AH, Bastian BC. From melanocytes to melanomas. *Nat. Rev. Cancer* 2016;**16**(6):345–58.

5 Bennett DC, Cooper PJ, Hart IR. A line of non-tumorigenic mouse melanocytes, syngeneic with the B16 melanoma and requiring a tumour promoter for growth. *Int. J. Cancer* 1987;**39**:414–18.

6 Oba-Shinjo SM, Correa M, Ricca TI, Molognoni F, Pinhal MA, Neves IA, et al. Melanocyte transformation associated with substrate adhesion impediment. *Neoplasia* 2006;**8**(3):231–41.

7 de Souza CF, Xander P, Monteiro AC, Silva AG, da Silva DC, Mai S, Bernardo V, Lopes JD, Jasiulionis MG. Mining gene expression signature for the detection of pre-malignant melanocytes and early melanomas with risk for metastasis. *PLos One* 2012;**7**(9):e44800.

8 Molognoni F, Jasiulionis MG. Epigenetics: A Possible Link Between Stress and Melanocyte Malignant Transformation. In: *Current Management of Malignant Melanoma*. Cao MY (Ed.) 11: 203-226 (2011), ISBN: 978-953-51-6498-2, IntechOpen

9 Tsoi J, Robert L, Paraiso K, Galvan C, Sheu KM, Lay J, Wong D, Atefi M, Shirazi R, Wang X, et al. Multi-stage differentiation defines melanoma subtypes with differential vulnerability to drug-induced iron-dependent oxidative stress. *Cancer Cell* 2018;**33**:890–904 e5.

10 Molognoni F, Cruz AT, Meliso FM, Morais AS, Souza CF, Xander P, Bischof JM, Costa FF, Soares MB, Liang G, et al. Epigenetic reprogramming as a key contributor to melanocyte malignant transformation. *Epigenetics* 2011;**6**(4):450–64.

11 de Souza CF. Assinaturas moleculares da progressão do melanoma. Sao Paulo (Brazil): Universidade Federal de São Paulo; 2013. p. 164.

12 Molognoni F, de Melo FH, da Silva CT, Jasiulionis MG. Ras and Rac1, frequently mutated in melanomas, are activated by superoxide anion, modulate Dnmt1

level and are causally related to melanocyte malignant transformation. *PLoS One* 2013;**8**(12):e81937.

13 Toricelli M, Melo FH, Peres GB, Silva DC, Jasiulionis MG. Timp1 interacts with beta-1 integrin and CD63 along melanoma genesis and confers anoikis resistance by activating PI3-K signaling pathway independently of Akt phosphorylation. *Mol. Cancer* 2013;**12**:22.

14 Monteiro AC, Muenzner JK, Andrade F, Rius FE, Ostalecki C, Geppert CI, Agaimy A, Hartmann A, Fujita A, Schneider-Stock R, et al. Gene expression and promoter methylation of angiogenic and lymphangiogenic factors as prognostic markers in melanoma. *Mol. Oncol.* 2019;**13**(6):1433–49.

15 Andrews S. FastQC: a quality control tool for high throughput sequence data. Available online at: http://www.bioinformatics.babraham.ac.uk/projects/fastqc. (2010)

16 Bolger AM, Lohse M, Usadel B. Trimmomatic: a flexible trimmer for Illumina sequence data. *Bioinformatics* 2014;**30**(15):2114–20.

17 Dobin A, Davis CA, Schlesinger F, Drenkow J, Zaleski C, Jha S, Batut P, Chaisson M, Gingeras TR. STAR: ultrafast universal RNA-seq aligner. *Bioinformatics* 2013;**29**(1):15–21.

18 Liao Y, Smyth GK, Shi W. The Subread aligner: fast, accurate and scalable read mapping by seed-and-vote. *Nucleic Acids Research* 2013;**41**:e108.

19 Ritchie ME, Phipson B, Wu D, Hu Y, Law CW, Shi W, Smyth GK. limma powers differential expression analyses for RNA-sequencing and microarray studies. *Nucleic Acids Res* 2015;**43**(7):e47.

20 Wickham H. *ggplot2: Elegant graphics for data analysis*, New York: Springer-Verlag; 2016. ISBN 978-3-319-24277-4.

21 Reimand J, Kull M, Peterson H, Hansen J, Vilo J. g:Profiler–a web-based toolset for functional profiling of gene lists from large-scale experiments. *Nucleic Acids Res* 2007;**35**(Web Server issue):W193–200.

22 Gautier L, Cope L, Bolstad BM, Irizarry RA. Affy—analysis of Affymetrix GeneChip data at the probe level. *Bioinformatics* 2004;**20**(3):307–15.

23 Pagès H, Carlson M, Falcon S, Li N. AnnotationDbi: Annotation Database Interface. R package version 1.40.0 (2017)

24 Nsengimana J, Laye J, Filia A, O'Shea S, Muralidhar S, Pożniak J, Droop A, Chan M, Walker C, Parkinson L, et al. β-Catenin-mediated immune evasion pathway frequently operates in primary cutaneous melanomas. *J. Clin. Invest.* 2018;**128**(5):2048–63.

25 Dahl C, Abildgaard C, Riber-Hansen R, Steiniche T, Lade-Keller J, Guldberg P. Kit is a frequent target for epigenetic silencing in cutaneous melanoma. *J. Invest. Dermatol.* 2015;**135**:516–24.

26 Bennett DC. Genetics of melanoma progression: the rise and fall of cell senescence. *Pigment Cell Melanoma Res* 2016;**29**(2):122–40.

27 Morais AS. Investigação de reguladores chaves da transição epitélio-mesênquima e do fenótipo stem cell-like em fases distintas da progressão do melanoma. Sao Paulo (Brazil): Universidade Federal de São Paulo; 2017. p. 142.

28 Zhang L, Yang M, Gan L, He T, Xiao X, Stewart MD, Liu X, Yang L, Zhang T, Zhao Y, et al. DLX4 upregulates TWIST and enhances tumor migration, invasion and metastasis. *Int. J. Biol. Sci.* 2012;**8**(8):1178–87.

29 Shakhova O, Zingg D, Schaefer SM, Hari L, Civenni G, Blunschi J, Claudinot S, Okoniewski M, Beermann F, Mihic-Probst D, et al. Sox10 promotes the formation and maintenance of giant congenital naevi and melanoma. *Nat. Cell. Biol.* 2012;**14**(8):882–90.

30 Hoek KS, Goding CR. Cancer stem cells versus phenotype-switching in melanoma. *Pigment Cell Melanoma Res* 2010;**23**:746–59.

31 Hoek KS, Eichhoff OM, Schlegel NC, Döbbeling U, Kobert N, Schaerer L, Hemmi S, Dummer R. In vivo switching of human melanoma cells between proliferative and invasive states. *Cancer Res* 2008;**68**(3):650–6.

32 Ahn A, Chatterjee A, Eccles MR. The slow cycling phenotype: a growing problem for treatment resistance in melanoma. *Mol. Cancer Ther.* 2017;**16**(6):1002–9.

33 Rambow F, Rogiers A, Marin-Bejar O, Aibar S, Femel J, Dewaele M, Karras P, Brown D, Chang YH, Debiec-Rychter M, et al. Toward Minimal Residual Disease-Directed Therapy in Melanoma. *Cell* 2018;**174**(4):843–55 e19.

34 Wickremesekera AC, Brasch HD, Lee VM, Davis PF, Woon K, Johnson R, Tan ST, Itinteang T. Expression of cancer stem cell markers in metastatic melanoma to the brain. *J. Clin. Neurosci.* 2019;**60**:112–16.

35 Marrot L, Jones C, Perez P, Meunier JR. The significance of Nrf2 pathway in (photo)-oxidative stress response in melanocytes and keratinocytes of the human epidermis. *Pigment Cell Melanoma Res* 2008;**21**(1):79–88.

36 Okubo A, Yasuhira S, Shibazaki M, Takahashi K, Akasaka T, Masuda T, Maesawa C. NAD(P)H dehydrogenase, quinone 1 (NQO1), protects melanin-producing cells from cytotoxicity of rhododendrol. *Pigment Cell Melanoma Res* 2016;**29**(3):309–16.

37 Campos AC, Molognoni F, Melo FH, Galdieri LC, Carneiro CR, D'Almeida V, Correa M, Jasiulionis MG. Oxidative stress modulates DNA methylation during melanocyte anchorage blockade associated with malignant transformation. *Neoplasia* 2007;**9**(12):1111–21.

38 Melo FH, Molognoni F, Morais AS, Toricelli M, Mouro MG, Higa EM, Lopes JD, Jasiulionis MG. Endothelial nitric oxide synthase uncoupling as a key mediator of melanocyte malignant transformation associated with sustained stress conditions, *Free Radic. Biol. Med.* 2011;**50**(10):1263–73.

39 Ricca TI, Liang G, Suenaga AP, Han SW, Jones PA, Jasiulionis MG. Tissue inhibitor of metalloproteinase 1 expression associated with gene demethylation confers *anoikis* resistance in early phases of melanocyte malignant transformation. *Transl. Oncol.* 2009;**2**(4):329–40.

40 Metri R, Mohan A, Nsengimana J, Pozniak J, Molina-Paris C, Newton-Bishop J, Bishop D, Chandra N. Identification of a gene signature for discriminating metastatic from primary melanoma using a molecular interaction network approach. *Sci. Rep.* 2017;**7**(1):17314.

41 Natali PG, Nicotra MR, Winkler AB, Cavaliere R, Bigotti A, Ulrich A. Progression of human cutaneous melanoma is associated with loss of expression of c-kit proto-oncogene receptor. *Int. J. Cancer* 1992;**52**:197–201.

42 Neiswender JV, Kortum RL, Bourque C, Kasheta M, Zon LI, Morrison DK, Ceol CJ. KIT Suppresses BRAF V600E-Mutant Melanoma by Attenuating Oncogenic RAS/MAPK Signaling. *Cancer Res* 2017;**77**(21):5820–30.

43 Pérez-Losada J, Sánchez-Martín M, Rodríguez-García A, Sánchez ML, Orfao A, Flores T, Dánchez-García I. Zinc-finger transcription factor Slug contributes to the function of the stem cell factor c-kit signaling pathway. *Blood* 2002;**100**:1274–86.

44 Bogeas A, Morvan-Dubois G, El-Habr EA, Lejeune FX, Defrance M, Narayanan A, Kuranda K, Burel-Vandenbos F, Sayd S, Delaunay V, et al. Changes in chromatin state reveal ARNT2 at a node of a tumorigenic transcription factor signature driving glioblastoma cell aggressiveness. *Acta Neuropathol* 2018;**135**(2):267–83.

45 Patel S, Wilkinson CJ, Sviderskaya EV. Loss of both CDKN2A and CDKN2B allows for centrosome overduplication in melanoma. *J. Invest. Dermatol* 2020 S0022-202X(20): 30147-0.

46 McNeal AS, Liu K, Nakhate V, Natale CA, Duperret EK, Capell BC, Dentchev T, Berger SL, Herlyn M, Seykora JT. CDKN2B Loss Promotes Progression from Benign Melanocytic Nevus to Melanoma. *Cancer Discov* 2015;**5**(10):1072–85.

47 Wu Z, Cheng K, Shi L, Li Z, Negi H, Gao G, Kamle S, Li D. Sal-like protein 2 upregulates p16 expression through a proximal promoter element. *Cancer Sci* 2015;**106**(3):253–61.

48 Silva AG, Graves HA, Guffei A, Ricca TI, Mortara RA, Jasiulionis MG, Mai S. Telomere-centromere-driven genomic instability contributes to karyotype evolution in a mouse model of melanoma. *Neoplasia* 2010;**12**(1):11–19.

49 Herbert K, Binet R, Lambert JP, Louphrasitthiphol P, Kalkavan H, Sesma-Sanz L, Robles-Espinoza CD, Sarkar S, Suer E, Andrews S, et al. BRN2 suppresses apoptosis, reprograms DNA damage repair, and is associated with a high somatic mutation burden in melanoma. *Genes Dev* 2019;**33**(5-6):310–32.

50 Brunner G, Reitz M, Schwipper V, Tilkorn H, Lippold A, Biess B, Suter L, Atzpodien J. Increased expression of the tumor suppressor PLZF is a continuous predictor of long-term survival in malignant melanoma patients. *Cancer Biother. Radiopharm.* 2008;**23**(4):451–9.

51 Felicetti F, Bottero L, Felli N, Mattia G, Labbaye C, Alvino E, Peschle C, Colombo MP, Carè A. Role of PLZF in melanoma progression. *Oncogene* 2004;**23**(26):4567–76.

52 Nishimura EK, Suzuki M, Igras V, Du J, Lonning S, Miyachi Y, Roes J, Beermann F, Fisher DE. Key roles for transforming growth factor beta in melanocyte stem cell maintenance. *Cell Stem Cell* 2010;**6**(2):130–40.

53 Howlin J, Cirenajwis H, Lettiero B, Staaf J, Lauss M, Saal L, Borg A, Gruvberger-Saal S, Jönsson G. Loss of CITED1, an MITF regulator, drives a phenotype switch in vitro and can predict clinical outcome in primary melanoma tumours. *PeerJ* 2015;**3**:e788.

54 Elworthy S, Lister JA, Carney TJ, Raible DW, Kelsh RN. Transcriptional regulation of mitfa accounts for the sox10 requirement in zebrafish melanophore development. *Development* 2003;**130**:2809–18.

55 Javelaud D, Alexaki VI, Pierrat MJ, Hoek KS, Dennler S, Van Kempen L, Bertolotto C, Ballotti R, Saule S, Delmas V, et al. GLI2 and M-MITF transcription factors control exclusive gene expression programs and inversely regulate invasion in human melanoma cells. *Pigment Cell Melanoma Res* 2011;**24**(5):932–43.